

IDENTIFICATION OF ANISOTROPIC ELASTIC MATERIAL PROPERTIES FROM MICRO-FEM SIMULATIONS FOR NATURAL MATERIALS

¹Ralf Schneider*, ²Ulrich Hindenlang, ¹Michael Resch

¹High Performance Computing Center Stuttgart (HLRS), Germany,

²LASSO Ingenieursgesellschaft mbH, Germany

KEYWORDS –

Cancellous bone; elastic material properties; Representative volume element RVE; micro CT

ABSTRACT –

Aim of this study is the determination of continuum elastic material properties for natural materials via direct numeric simulation of the material's micro structure. The subject matter to this study and an example for a natural material is cancellous bone.

The calculation procedure which is based on the so called direct mechanics approach is applied to a cube shaped bone specimen taken from the knee joint region of a human femur.

The bone specimen of approximately 8mm edge length was scanned with a micro computer tomograph with 0,014mm isotropic spatial resolution. From this dataset a high resolution FEM model was created.

As a start the procedure is applied to the model in its original size. The results will be shown and discussed in detail to demonstrate their plausibility. Further on the model will be divided into sub domains and the procedure is then applied to each domain. By means of these results the influence of the chosen RVE size to the derived continuum elastic material properties will be shown.

TECHNICAL PAPER -

1. INTRODUCTION

The biomechanical simulation of bone-implant systems is subject to many studies presented in the open literature. Up to the present day most of these studies consider bone tissue as an isotropic material with inhomogeneous distribution throughout the model even though it is also well proven that especially cancellous bone, which fills the joint region of the long bones has to be considered at least as orthotropic [1, 2, 3, 4].

The negligence of the correct material properties can be assigned to their minor influence to global solutions in contrast to, for example, the muscle forces. Another problem is the non-existence of proper material models which provide a suitable mapping of orthotropic inhomogeneous material distributions from clinical imaging data to FE-models.

The existence of correlations between bone density data which are provided for example by clinical computer tomography and orthotropic elastic constants for bone is shown in [5].

That these experimentally determined correlations can be utilized in an engineering manner to generate orthotropic inhomogeneous material distributions from clinical CT-data suitable for FE-simulations is shown by Schneider et al. [6].

A question which arises from this kind of material mappings and also from the general application of the FE method with elastic continuum material formulations to micro structured natural materials is the one of resolution.

With clinical computer tomography isotropic spatial resolutions up to 0.5mm are possible. The element length in currently used FE-models for the simulation of bone implant systems, for example of the human femur, varies between 1mm – 3mm [2, 7, 8].

For the experimental determination of elastic constants specimens with an edge length of approximately 10mm are used [9, 10].

The current mapping method proposed by our group calculates the elastic constants by averaging all voxels of a CT dataset which are enclosed in one element of the corresponding FE-mesh. This means the resulting representative volume element (RVE) is equal to the element resolution of the FE mesh but not even close to the size of the RVE used to determine the elastic constants from experiments.

If one now wants to do non-linear simulations which include plasticity and damage models a refinement of the FE-meshes close to the implant will be necessary what of course will lead to a further decrease of the RVE size.

The aim of this study is to evaluate the influence of the RVE size reduction to the elastic material constants by means of the direct mechanics approach. Also this study is a first step towards the clarification whether it is justified to apply an orthotropic continuum material model to bone tissue if the RVE size decreases to the resolution of clinical imaging data.

2. MATERIALS AND METHODES

In this part the theoretical methods applied to bone specimens as well as the specimen itself and the modelling techniques used for the geometry setup are described.

Averaged quantities of the RVE will be noted with a bar accent, tensor quantities are noted in non italic font and matrix quantities are noted in bold, big letters.

If not specified the indices of all quantities are $\in [1,2,3]$ and the Einstein summation convention has to be applied if indices appear in equal pairs.

Standard mechanics approach

With the standard mechanics approach a procedure is described which is often used as the starting point to the application of homogenisation theory [11, 12]. Aim of the approach is the determination of averaged elastic properties of micro structured materials on the continuum level. One prerequisite which is essential to this approach is that the material properties of the microstructures in the analysed RVE are known. In this study the material of the bone microstructures is considered to be homogeneous with isotropic behaviour.

To calculate the averaged macroscopic strain in an RVE from the local microscopic strain in the microstructures, the connection

$$\bar{\epsilon}_{ij} = \frac{1}{|V_{RVE}|} \int_{V_{RVE}} \epsilon_{ij} dV_{RVE} = \frac{1}{|V_{RVE}|} \int_{S_{RVE}} \frac{1}{2} (u_i n_j + u_j n_i) dS_{RVE} \quad (1)$$

is given, with:

V_{RVE} , S_{RVE} the Volume and the Boundary of the RVE respectively;

$\bar{\epsilon}_{ij}$ the mean strain tensor of the RVE;

ϵ_{ij} the local strain tensor;

u_i the prescribed displacement on the RVE boundary;

n_j the normal vector to the RVE boundary.

A similar connection is given for the calculation of the averaged macroscopic stress in the RVE from the local microscopic stresses.

$$\bar{\sigma}_{ij} = \frac{1}{|V_{RVE}|} \int_{V_{RVE}} \sigma_{ij} dV_{RVE} = \frac{1}{|V_{RVE}|} \int_{S_{RVE}} \frac{1}{2} (\bar{t}_i \gamma_j + \bar{t}_j \gamma_i) dS_{RVE} \quad (2)$$

With:

$\bar{\sigma}_{ij}$ the mean stress tensor of the RVE;

σ_{ij} the local stress tensor;

\bar{t}_i the prescribed traction on the RVE boundary;

γ_j a local coordinate on the RVE boundary.

To connect the averaged macroscopic strain applied to the RVE with the resulting averaged macroscopic stress one defines

$$\bar{\sigma}_{ij} = \bar{C}_{ijkl} \bar{\epsilon}^{kl} \quad (3)$$

With \bar{C}_{ijkl} the so called effective stiffness of the RVE which is a tensor of rank four.

Furthermore, to connect the local microscopic strains with the averaged macroscopic strain the local structure tensor M_{ijkl} , also a tensor of rank four, is defined by

$$\epsilon_{ij} = M_{ijkl} \bar{\epsilon}^{kl} \quad (4)$$

The development of the correlation between the elastic properties of the microscopic structures to the averaged elastic properties of the RVE is started from the generalised Hooke's law on the microscopic level

$$\sigma_{ij} = C_{ijkl} \epsilon^{kl} \quad (5)$$

Integrating both sides of equation (5) yields

$$\frac{1}{|V_{RVE}|} \int_{V_{RVE}} \sigma_{ij} dV_{RVE} = \frac{1}{|V_{RVE}|} \int_{V_{RVE}} C_{ijkl} \epsilon^{kl} dV_{RVE} \quad (6)$$

Substituting the left hand side with equation (2) and ϵ^{kl} with equation (4) we get

$$\bar{\sigma}_{ij} = \frac{1}{|V_{RVE}|} \int_{V_{RVE}} C_{ijmn} M^{mn}_{kl} dV_{RVE} \bar{\epsilon}^{kl} \quad (7)$$

Comparing equation (7) to equation (3) one recognizes the relation

$$\bar{C}_{ijkl} = \frac{1}{|V_{RVE}|} \int_{V_{RVE}} C_{ijmn} M^{mn}_{kl} dV_{RVE} \quad (8)$$

from which the effective stiffness of the RVE can be calculated if the local elastic properties and the function of the local structure tensor for the micro structure of the RVE are known.

Due to symmetries in the local stiffness tensor and the local structure tensor equation (8) can be rewritten as a 6 x 6 matrix equation in terms of the averaged and local stiffness matrices $\bar{\mathbf{E}}$, \mathbf{E} and the local structure matrix \mathbf{A}

$$\bar{\mathbf{E}} = \frac{1}{|V_{RVE}|} \int_{V_{RVE}} \mathbf{E} \mathbf{A} dV_{RVE} \quad (9)$$

The change from the tensor indices $\in [1,2,3]$ to the matrix indices $\in [1,2,\dots,6]$ is done as follows

$$11 = 1, \quad 22 = 2, \quad 33 = 3, \quad 12 = 21 = 4, \quad 13 = 31 = 5, \quad 23 = 32 = 6$$

To calculate the local structure matrix equation (4) is also rewritten in terms of the local structure matrix \mathbf{A} and the averaged and local strain vectors $\bar{\boldsymbol{\varepsilon}}$ and $\boldsymbol{\varepsilon}$ of dimension 6 x 1

$$\boldsymbol{\varepsilon} = \mathbf{A} \bar{\boldsymbol{\varepsilon}} \quad (10)$$

To solve equation (10) for a cube shaped RVE each column of \mathbf{A} is calculated separately from one of six load cases which are applied to the RVE. From these six load cases are three pure compression and three pure shear loads.

So for the load case s the components of the average strain tensor $\bar{\boldsymbol{\varepsilon}}_s$ are:

$$\begin{aligned} \bar{\varepsilon}_{rr} &= \frac{1}{3} \Leftrightarrow r = s \\ \bar{\varepsilon}_{rs} &= 0 \Leftrightarrow r \neq s \end{aligned} \quad \text{with } r, s \in [1, \dots, 6]$$

From that technique we get

$$\mathbf{A} = \sum_{s=1}^6 \mathbf{A}_s = \sum_{s=1}^6 \boldsymbol{\varepsilon}_s \cdot \bar{\boldsymbol{\varepsilon}}_s^T \quad (11)$$

Summarizing the described procedure one has to do the following steps

1. Apply the six described load cases to the FE model of the analysed RVE
2. Calculate the local structure matrix \mathbf{A} for each element according to equ. (11)
3. Integrate the effective stiffness of the RVE according to equ. (9)

Determination of material symmetries

Since this study deals with natural materials material symmetries in the analysed specimens cannot be known a priori and so the calculated effective stiffness matrices will be dense in general.

To determine whether there are distinguished directions in which material symmetries like orthotropy appear, the calculated effective stiffness tensors were simply transformed step by step with a rotating coordinate system. The coordinate system was rotated with its third direction over a complete hemisphere and according to each rotation step of the third direction the first and second direction was rotated over an angle of π . See fig. 1 for the definition of the rotation angles.

For each transformation of the effective stiffness tensor the sum of squares of the coupling terms being 0 for an ideal symmetric material was evaluated.

$$E_{14}^2 + E_{15}^2 + E_{16}^2 + E_{24}^2 + E_{25}^2 + E_{26}^2 + E_{34}^2 + E_{35}^2 + E_{36}^2 + E_{45}^2 + E_{46}^2 + E_{56}^2 = \min \quad (12)$$

The minimum of these sums was then assigned the highest achievable symmetry in the material properties of the analysed RVE.

The advantage of this approach over its low efficiency and also over the possible application of optimisation algorithms are its simplicity in implementation and that the global minimum of equation (12) will always be found.

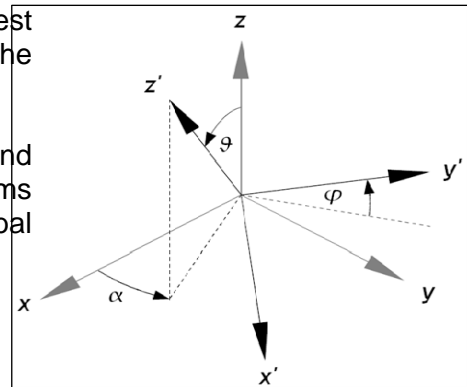


Figure 1 – Rotation angles

Bone specimens

The subject matter of this study was a micro computer tomography data set taken of a cancellous bone specimen from the distal joint region of a cadaverous, primed human femur (see fig. 2). The physical dimension of the specimen was 10mm cubed.

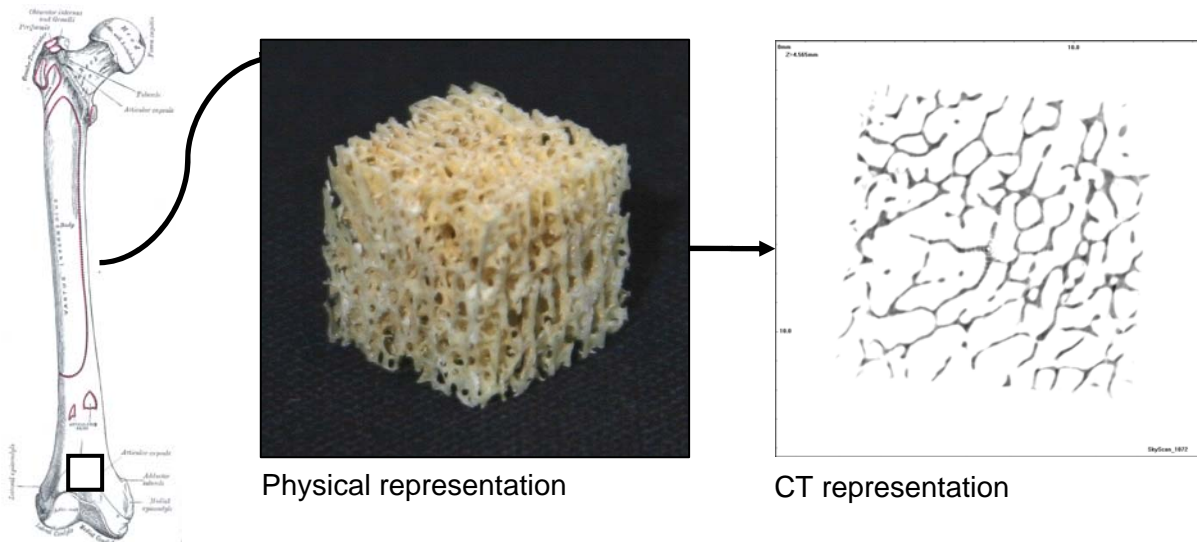


Figure 2 – Position and representations of cancellous bone specimen

The size of the micro-CT data set was 817 x 865 x 504 voxels with an isotropic special resolution of 0.014mm.

To avoid the disturbance from the cutting blade in the boundary regions of the specimen only 350 voxels in each direction were used from the original data set which results in a physical cube shaped model with an edge length of $l = 4.9\text{mm}$.

Finite-Element models

For the extraction of the bone geometry from the CT data the iso-surface module from the HLRS visualisation tool COVISE was used. The module triangulates iso-surfaces by means of the marching-cubes algorithm. The output is then written as an ABAQUS input deck which makes it possible to directly import the bone geometry on triangle basis into ANSA.

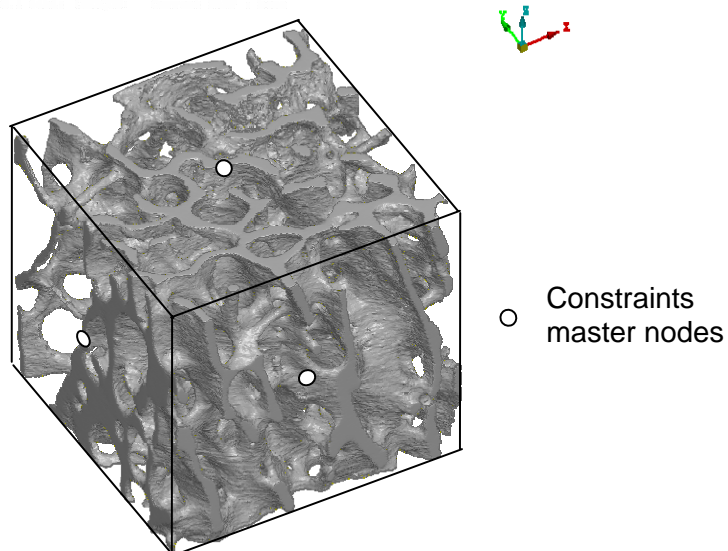


Figure 3 – Geometry configuration of complete modelled volume

Since the marching cubes algorithm produces triangles of bad quality not suitable for direct FE-meshing a mesh reconstruction was performed with ANSA. Also the element edge length was increased during the reconstruction from 0.014mm to 0.03mm to reduce the total number of triangles. A further coarsening of the mesh was not applied since the reconstruction produced topological errors in the surface mesh which had to be fixed manually. The finally modelled geometry is shown in fig. 3.

After mesh reconstruction and improvement the bone geometry was split in 8 sub-volumes each with an edge length of $l = 2.45\text{mm}$ (see fig. 4). The sub-volumes are specified by indices according to their position on the coordinate axes, e.g. the one next to the origin of the coordinate system in the lower left corner is called SV_{x-y-z} .

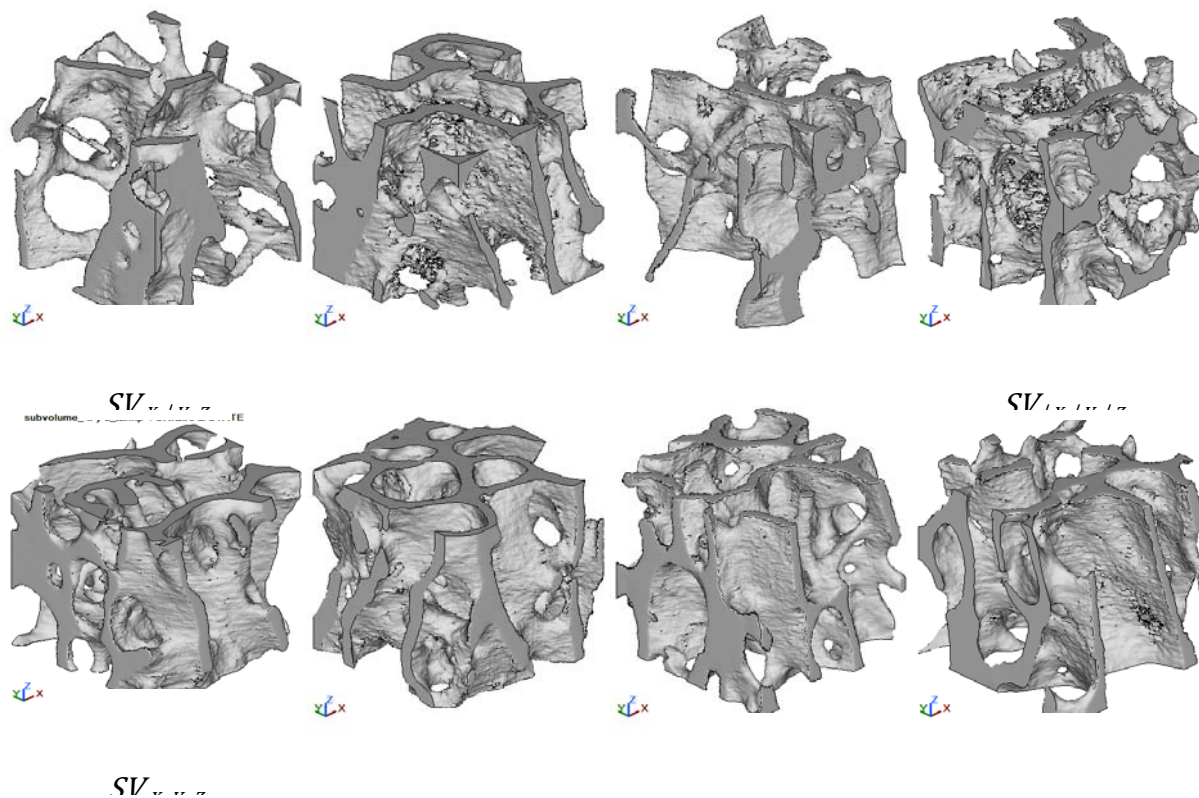


Figure 4 – Geometry configuration of sub-volumes

The boundary conditions for applying the six load cases were modelled with ABAQUS constraints as follows. One independent master node was placed in the middle of each face of the considered volume cube. Then the degree of freedom (DOF) of all nodes in one face acting in the normal direction of the face was coupled to the rigid body movements of the corresponding master node. This technique allows a free movement of all nodes in one face in tangential directions while ensuring that the face remains absolutely planar.

The prescribed displacements can now simply be placed on the six master nodes, translational as well as rotational ones, so reproducing the desired average strains needed for the evaluation of equ. (11). The DOFs of the according master nodes which are applied with prescribed displacements are listed in tab. 1 for each face of the volume cube.

Cube faces	Normals of cube faces	DOFs with prescribed displ.
xy	[-1 0 0] / [1 0 0]	3, 4, 5
xz	[0 -1 0] / [0 1 0]	2, 4, 6
yz	[0 0 -1] / [0 0 1]	1, 5, 6

Table 1 – DOFs with prescribed displacements for cube faces

The boundary conditions applied for each load case are summarised in tab. (2). The load cases are specified by the according strain they are inducing in the considered volume. To all DOFs which are listed for a face in tab. 1 but not being specified in column 4 of tab. 2 a prescribed displacement of 0 was applied.

Load case	Displ. cube face	Normal of displ.cube face	Displaced DOF	Induced strain $\frac{\Delta l}{l}$
xx	yz	[1 0 0]	1	-0.001
yy	xz	[0 1 0]	2	-0.001
zz	xy	[0 0 1]	3	-0.001
xy	yz	[-1 0 0]	6	-0.001
	yz	[1 0 0]	6	
xz	yz	[-1 0 0]	5	0.001
	yz	[1 0 0]	5	
yz	xz	[0 -1 0]	4	-0.001
	xz	[0 1 0]	4	

Table 2 – Specification of prescribed displacements for load cases

As already mentioned the FE simulations done for this study were carried out with ABAQUS 6.8-4. The homogeneous isotropic material applied to the bone structures was modelled with the elastic constants $E_{iso} = 5330 \text{ MPa}$ and $\nu_{iso} = 0.3$ according to [13].

The calculations of the effective stiffness matrices and the search for possible symmetries of the material constants were done with a post processing procedure implemented and developed in FORTRAN 2003 and Coarray FORTRAN at the HLRS.

3. RESULTS

Below the evaluations of the calculated effective stiffness matrices are presented. When in this part it is spoken from “symmetry directions” the normals of the major symmetry planes of a material are meant.

Absolute value of the effective stiffness matrix coefficients

First the absolute values of the components E_{ij} of the calculated effective stiffness matrices \mathbf{E}

are evaluated. Before the evaluation was done, all matrices were transformed so that E_{11} is

the lowest and E_{33} is the highest of the three normal stiffness components.

In fig. 5 the absolute value of E_{11} and E_{33} , the highest and lowest shear stiffness components,

denoted with $E_{S,min}$ and $E_{S,max}$, and the highest coupling term, denoted with $E_{C,max}$, which should

be zero in the case of a material with 3 or more major symmetry planes, are presented.

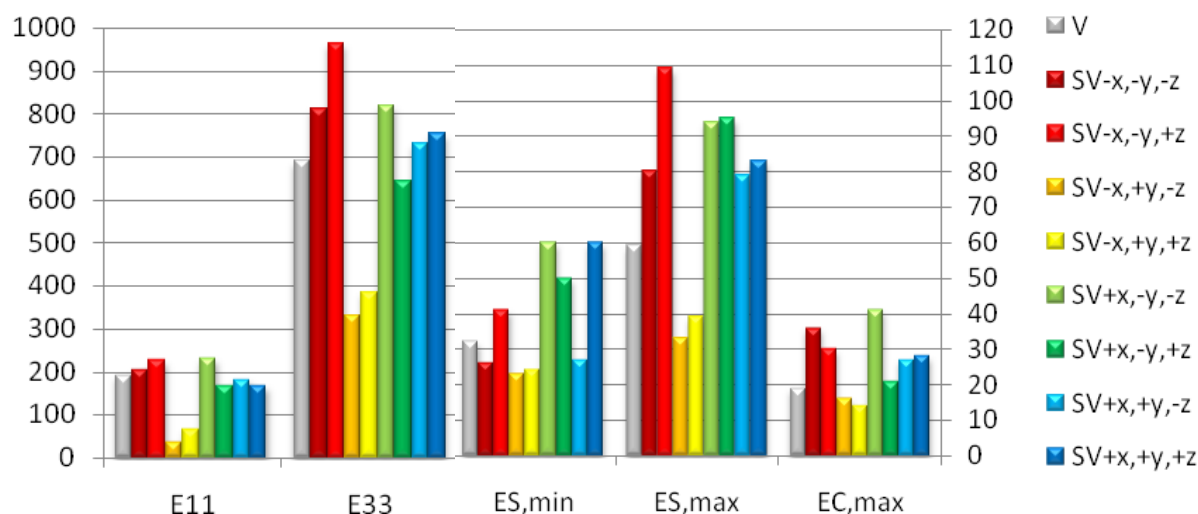


Figure 5 – Absolute values of selected stiffness components

The first result that can be seen is, that the values of the calculated normal and shear stiffness coefficients are comparable to the ones that can be found in the literature for cancellous bone [13].

Regarding the problem of resolution, from fig. 5 it can further be seen that the increase of resolution from 4.9mm to 2.45mm reveals a significant variance of the elastic coefficients in

V. The effective stiffness matrices calculated for V and all sub-volumes can be found in

annex A.

There the reader can also see that all calculated matrices are completely symmetric which proves, that the boundary conditions specified in the last section are consistent.

Difference between calculated and expected material behaviour

The major characteristic of orthotropic material behaviour is the decoupling of normal and shear strains if the material coordinate system is oriented along the three orthogonal, distinguished material directions. This means, that only the non diagonal coefficients of the stiffness matrix, which couple normal to normal strains, are $\neq 0$.

To specify the difference between the calculated effective material behaviour and the expected orthotropic material behaviour Δc the sum of absolute values of the shear to normal strain coupling coefficients normalised with respect to the highest normal to normal strain coupling coefficient in the considered matrix is evaluated.

As an example for this approach the evaluation for E_V is shown below.

$$E_V = \begin{bmatrix} 192 & 71 & 104 & 17 & 4 & 1 \\ 71 & 245 & 95 & 0 & 7 & 19 \end{bmatrix} \rightarrow \begin{bmatrix} 0,234 & 0,060 & 0,016 \\ 0,001 & 0,093 & 0,266 \end{bmatrix}$$

$\Delta o_V = 0.890$

The comparison of E_V and the sub-volumes can be seen in fig. 6.

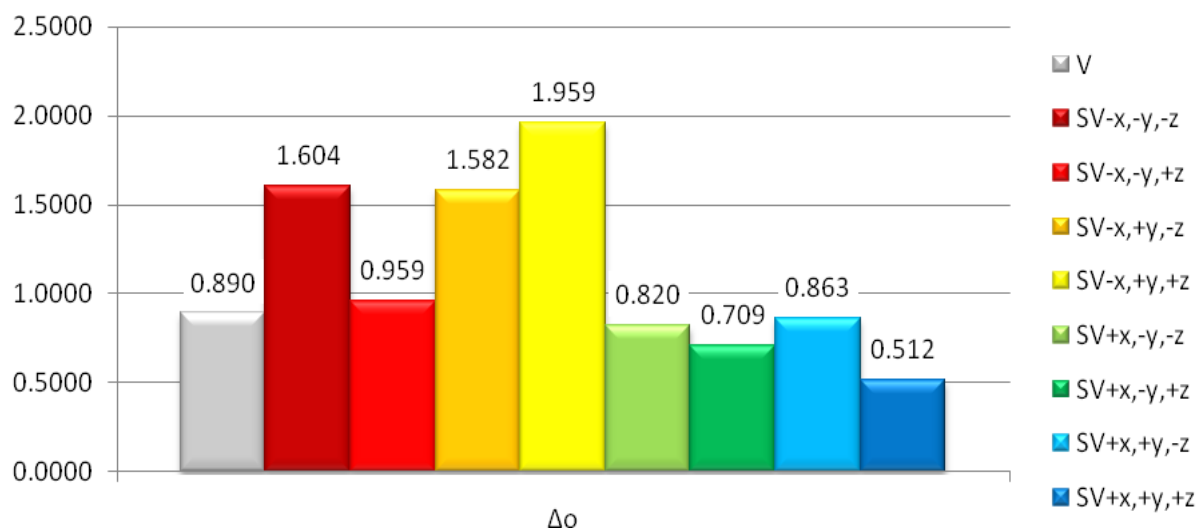


Figure 6 – Absolute values of selected stiffness components

What can be seen from fig. 6 is the fact that not only the absolute values of the stiffness coefficients show variations when increasing the resolution but also the degree of orthotropy

in 4 out of the eight sub-volumes is significantly different from the one of V .

The authors are aware, that from the analysis of one specimen no general conclusions can

be drawn. But looking at the total values of ΔO_V and ΔO_{SV} one can recognize the tendency that

a material model made for a lower resolution scale is not necessarily valid for a higher one. Another tendency which can be seen in the analysis of the elastic constants is that the difference to the general assumption of bone material being fully orthotropic is increasing with the level of resolution.

Directions of major material symmetries

The evaluation of the coordinate systems which were found with the search for the minimum of the shear to normal strain coupling coefficients showed that the orientation of the highest normal

stiffness coefficient is not significantly different in V and six of its

sub-volumes. Here the 33-direction is oriented up to the difference of some degrees along the global zz-direction.



Figure 7 – Main load trajectories

This orientation is the one which was expected at least for V since

the specimen was indeed cut from an arbitrary position in the knee joint region of the bone but the axes of the cube were oriented along the main load trajectories.

These load trajectories can be found in most joint regions of long bones. They are oriented during the remodelling process of bone tissue towards the directions in which the main loads to the bone are acting (see fig. 7).

In fig. 8 the orientations of V and all sub-volumes are shown with their correct relative position to each other.

What was not expected and kind of surprising in this evaluation is the fact, that in the two

sub-volumes $SV_{+x,-y,-z}$ and $SV_{+x,+y,-z}$ the general orientation of the major symmetry directions is

still similar to the ones of V and the other sub-volumes but the 11- and 33-direction have switched places.

Looking at the orientations of the 11- and 22-direction it can be seen, that only the ones in

$SV_{-x,-y,-z}$ and $SV_{-x,y,+z}$ are oriented similar than the one in V .

This result suggests that not only the variance of the elastic coefficients with the level of resolution but also the variance of the orientation of the major symmetry directions has to be analysed on the correct resolution level.

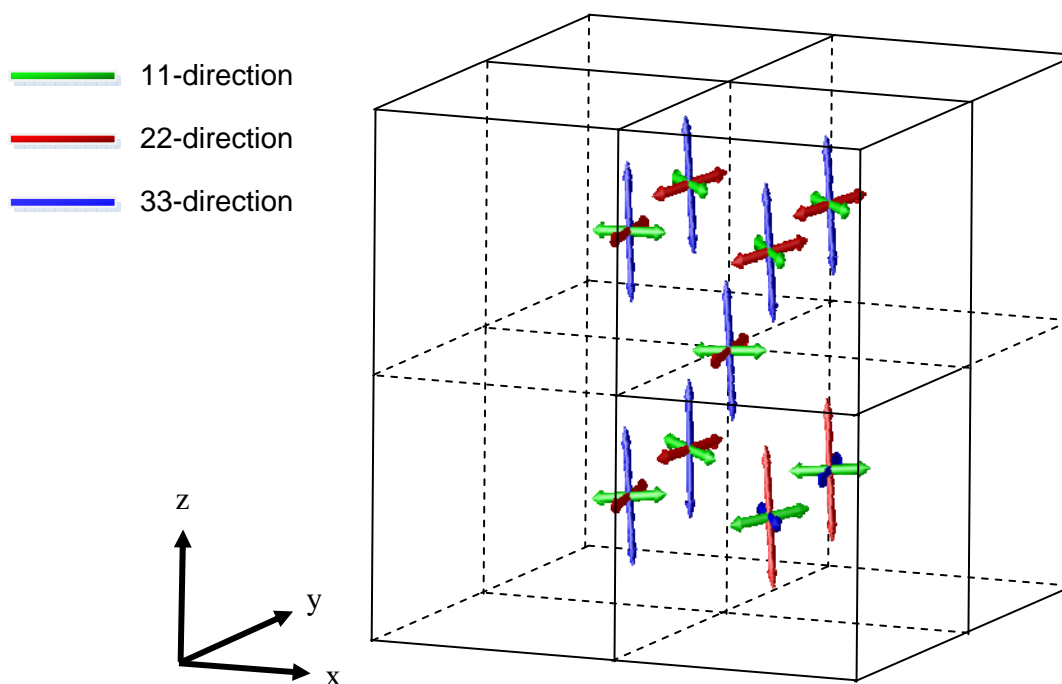


Figure 8 – orientations of the major symmetry directions.

This result is essential to the application of material mapping methods like the one proposed in [6] because there the calculation of the material constants from the scalar field of the CT density data is independent from the algorithm which determines the orientation of the material symmetry directions.

This means only if this algorithm considers the CT data with the same resolution as the calculation of the material constants does, the mapping method will produce consistent material data.

4. CONCLUSIONS

In this study the standard mechanics approach for the calculation of the effective stiffness matrices of micro structured materials was applied to a cancellous bone specimen at two different RVE resolutions. The resolutions are both significantly smaller than the ones which are used in the literature for the experimental determination of elastic material constants

where the resolution with the smaller RVE size was comparable to the one which is used as the mesh resolution in current FE simulations of bone-implant-systems.

It was shown, that on this RVE scale the general assumption of bone material being orthotropic has to be handled with care, since the normal- to shear strain coupling coefficient are already of significant size compared to the normal to normal strain coupling components.

Furthermore the evaluation of the orientation of the major symmetry planes in the analysed RVEs showed that there are also variances with increasing resolution. The effect was more observable between the local 11- and 22-directions than between the local 33-directions but nonetheless two out of eight sub-volumes showed a significantly different orientation than the others.

As already mentioned it is clear to the authors that from the analysis of one bone specimen one can't draw any general conclusions, but we think one can say that the results of this study reveal a dependency of the local material constants upon the used RVE size. Furthermore we think that resolution currently used for the FE simulation of bone implant systems lies in a not very lucky range where the statement can be made:

“The increase of resolution goes along with a decrease of material symmetry”

For future development it is planned to fully automate the developed semi-automatic model setup and evaluation procedures so that they can efficiently be applied to a larger number of bone specimens.

Also more than two resolution steps will be evaluated to make the transition, from orthotropic material behaviour on the continuum level to isotropic behaviour on the micro structural level, visible.

Both points are meant to confirm the statements and observations made during this study.

REFERENCES

- (1) Validation of subject-specific automated p-FE analysis of the proximal femur, N. Trabelsi, Z. Yosibash, C. Milgromb, *Journal of Biomechanics*, 42 (2009) 234-241
 - (2) A modified method for assigning material properties to FE models of bones, Benedikt Helgason, Fulvia Taddei, et al. *Medical Engineering & Physics* 30 (2008) 444-453
 - (3) Evaluation of orthogonal mechanical properties and density of human trabecular bone from the major metaphyseal regions with materials testing and computed tomography, M.J. Ciarelli, S.A. Goldstein, J.L. Kuhn, et al., *J. Orthop. Res.* 9 (1991) 674-682
 - (4) Ultrasonic measurement of orthotropic elastic constants of bovine femoral bone, W.C. Van Buskirk, S.C. Cowin, R.N. Ward, *J. Biomech. Engrg.* 103 (2) (1981) 67-72
 - (5) Relations of mechanical properties to density and CT numbers in human bone, J.Y. Rho, M.C. Hobatho, R.B. Ashman, *Med. Engrg. Phys.* 17 (1995) 347-355
 - (6) Inhomogeneous, orthotropic material model for the cortical structure of long bones modelled on the basis of clinical CT or density data, R. Schneider, G. Faust, U. Hindenlang, P. Helwig, *Comput. Methods Appl. Mech. Engrg.* 198 (2009) 2167-2174
 - (7) Finite element analysis of a bone-implant system with the proximal femur nail, P. Helwig, G. Faust, U. Hindenlang, B. Kröplin, C. Eingartner, *Technol. Health Care*
-

14 (2006) 411-419.

- (8) A standardized finite element model of the human femur for biomechanical simulations of proximal fractures,
S. Eberle, P. Augat, in: 14th Finite Element Workshop, University of Ulm, July 2007, ISBN:978-3-9806183-9-7, pp. 98-102
- (9) Estimation of mechanical properties of cortical bone by computed tomography,
S. Snyder, E. Schneider, J. Orthop. Res. 9 (1990) 422-431
- (10) Elastic modulus of trabecular bone material,
R.B. Ashman, J.Y. Rho, J. Biomech. 21 (3) (1988) 177-181
- (11) Elastic properties of reinforced solids: Some theoretical principles.
R. Hill, J. Mech. Phys. Solids 11 (1963) 357-372
- (12) A comparison of homogenization and standard mechanics analysis for periodic porous composites,
S.J. Hollister, N. Kikuchi, Computational Mechanics 10 (1992) 73-95
- (13) Direct mechanics assessment of elastic symmetries and properties of trabecular bone architecture,
B. van Rietbergen et al., J. Biomechanics 29 (12) (1996) 1653-1657

A. CALCULATED EFFECTIVE STIFFNESS MATRICES

$$\begin{bmatrix} 192 & 71 & 104 & 17 & 4 & 1 \\ 71 & 245 & 95 & 0 & 7 & 19 \end{bmatrix} \mathbf{E}_V =$$

$$\begin{bmatrix} 206 & 63 & 113 & 13 & -14 & 2 \\ 63 & 310 & 118 & 0 & -10 & -36 \end{bmatrix} \mathbf{E}_{SV-x,y,z} =$$

$$\begin{bmatrix} 227 & 106 & 139 & 18 & -23 & -5 \\ 106 & 423 & 162 & 0 & -12 & -30 \end{bmatrix}$$

$$\mathbf{E}_{SV-x,-y,+z} =$$

$$\begin{bmatrix} 38 & 39 & 30 & 0 & 4 & 5 \\ 39 & 134 & 47 & -4 & 7 & 16 \end{bmatrix}$$

$$\mathbf{E}_{SV-x,+y,-z} =$$

$$\begin{bmatrix} 67 & 51 & 28 & -11 & 9 & 2 \\ 51 & 110 & 47 & -5 & 4 & 14 \end{bmatrix}$$

$$\mathbf{E}_{SV-x,+y,+z} =$$

$$\begin{bmatrix} 231 & 162 & 102 & 41 & 5 & -5 \\ 162 & 311 & 141 & -2 & -4 & -21 \end{bmatrix}$$

$$\mathbf{E}_{SV+x,-y,-z} =$$

$$\begin{bmatrix} 167 & 141 & 81 & 0 & -3 & 10 \\ 141 & 240 & 117 & -1 & 4 & 1 \end{bmatrix}$$

$$\mathbf{E}_{SV+x,-y,+z} =$$

$$\begin{bmatrix} 183 & 88 & 83 & 27 & 14 & 7 \\ 88 & 274 & 117 & 0 & 0 & -1 \end{bmatrix}$$

$$\mathbf{E}_{SV+x,+y,-z} =$$

$$\begin{bmatrix} 168 & 136 & 123 & 2 & -4 & 8 \\ 136 & 236 & 136 & 4 & 0 & 28 \end{bmatrix}$$

$$\mathbf{E}_{SV+x,+y,+z} =$$